Magnetic Resonance Imaging 63 (2019) 29–36

Contents lists available at ScienceDirect

Magnetic Resonance Imaging

journal homepage: www.elsevier.com/locate/mri

Original contribution

T_1 and T_2^* mapping of the human quadriceps and patellar tendons using ultra-short echo-time (UTE) imaging and bivariate relaxation parameter-based volumetric visualization

M. Krämer[a,*,1], M.B. Maggioni[a,1], N.M. Brisson[b], S. Zachow[c], U. Teichgräber[d], G.N. Duda[b], J.R. Reichenbach[a]

[a] Medical Physics Group, Institute of Diagnostic and Interventional Radiology, Jena University Hospital, Friedrich Schiller University Jena, Germany
[b] Julius Wolff Institute and Center for Musculoskeletal Surgery, Charité – Universitätsmedizin Berlin, Germany
[c] Zuse Institute Berlin, Germany
[d] Institute of Diagnostic and Interventional Radiology, Jena University Hospital, Friedrich Schiller University Jena, Germany

ARTICLE INFO

Keywords:
UTE
Tendons
Patellar ligament
Segmentation
3D visualization

ABSTRACT

Quantification of magnetic resonance (MR)-based relaxation parameters of tendons and ligaments is challenging due to their very short transverse relaxation times, requiring application of ultra-short echo-time (UTE) imaging sequences. We quantify both T_1 and T_2^* in the quadriceps and patellar tendons of healthy volunteers at a field strength of 3 T and visualize the results based on 3D segmentation by using bivariate histogram analysis. We applied a 3D ultra-short echo-time imaging sequence with either variable repetition times (VTR) or variable flip angles (VFA) for T_1 quantification in combination with multi-echo acquisition for extracting T_2^*. The values of both relaxation parameters were subsequently binned for bivariate histogram analysis and corresponding cluster identification, which were subsequently visualized. Based on manually-drawn regions of interest in the tendons on the relaxation parameter maps, T_1 and T_2^* boundaries were selected in the bivariate histogram to segment the quadriceps and patellar tendons and visualize the relaxation times by 3D volumetric rendering. Segmentation of bone marrow, fat, muscle and tendons was successfully performed based on the bivariate histogram analysis. Based on the segmentation results mean T_2^* relaxation times, over the entire tendon volumes averaged over all subjects, were 1.8 ms ± 0.1 ms and 1.4 ms ± 0.2 ms for the patellar and quadriceps tendons, respectively. The mean T_1 value of the patellar tendon, averaged over all subjects, was 527 ms ± 42 ms and 476 ms ± 40 ms for the VFA and VTR acquisitions, respectively. The quadriceps tendon had higher mean T_1 values of 662 ms ± 97 ms (VFA method) and 637 ms ± 40 ms (VTR method) compared to the patellar tendon. 3D volumetric visualization of the relaxation times revealed that T_1 values are not constant over the volume of both tendons, but vary locally. This work provided additional data to build upon the scarce literature available on relaxation times in the quadriceps and patellar tendons. We were able to segment both tendons and to visualize the relaxation parameter distributions over the entire tendon volumes.

1. Introduction

Patellar tendinopathy often affects athletes of various disciplines and is mainly caused by tendon overuse, although the origin of the pathology is still incompletely understood [1]. Thus, insight into the MR relaxation properties of tendons and ligaments may be highly valuable to detect and potentially understand possible pathological developments due to the intricate interplay between water molecules and tendon tissue [2]. Conventional MR imaging protocols commonly applied in clinical practice are typically only able to detect later stages of the diseases, as direct imaging of ligaments and tendons by means of magnetic resonance imaging (MRI) is challenging due to the short T_2^* relaxation times in compact tissues, typically ranging between 0.5 ms and 2.5 ms [3–6]. With such fast decaying transverse magnetizations,

* Corresponding author at: Medical Physics Group, IDIR, Jena University Hospital, Philosophenweg 3, D-07443 Jena, Germany.
E-mail addresses: martinkraemer84@gmail.com (M. Krämer), marta.maggioni@uni-jena.de (M.B. Maggioni), nicholas.brisson@charite.de (N.M. Brisson), zachow@zib.de (S. Zachow), ulf.teichgraeber@med.uni-jena.de (U. Teichgräber), georg.duda@charite.de (G.N. Duda), Juergen.Reichenbach@med.uni-jena.de (J.R. Reichenbach).
[1] Both authors contributed equally.

https://doi.org/10.1016/j.mri.2019.07.015
Received 11 April 2019; Received in revised form 8 July 2019; Accepted 23 July 2019

tendons and ligaments appear characteristically black with no measurable signal on the images when data are acquired with conventional MRI sequences. However, with recent advances in ultra-short echo-time (UTE) imaging sequences, direct imaging of tendons has become possible, offering the possibility to quantify their relaxation parameters. Typically, UTE imaging sequences use 2D half pulses [7,8] or non-selective short rectangular radiofrequency (rf) pulses [9–12] for excitation to achieve echo times (TE) below 1 ms. With the introduction of UTE sequences, interest in the quantitative analysis of tendons tissues has been steadily increasing. Previous studies have demonstrated relevant changes in the T_2^* relaxation time as a consequence of loading [13], disease (e.g., diagnosed patellar tendinopathy [6]) and physical activity [14]. While the relevance of identifying changes of T_1 [5] is currently still under discussion, this work nevertheless explores the possibility of creating a single imaging protocol to quantify both parameters, T_2^* and T_1.

Various methods have been proposed to quantify T_1 relaxation time constants. Most methods combine an inversion pulse with fast low-angle shot (FLASH) or spin-echo based acquisition modules [15–17]. With UTE imaging, however, applying any spin-echo based technique in tissues with very short T_2/T_2^* relaxation times is challenging because the necessary time span between excitation and formation of a spin-echo initiated by the refocusing rf-pulse is usually too long. Furthermore, combining 3D-UTE imaging with hard pulse excitation, as used in this study, with an inversion pulse is not convenient because truly inverting short T_2^* components is challenging and total acquisition time would be considerably increased. For these reasons, estimation of T_1 with UTE sequences typically applies either the variable flip angle (VFA) [18,19] or the variable repetition time (VTR) [20] technique. Both methods exploit the fact that the steady state magnetization of a gradient-echo FLASH based UTE sequence can be deliberately modified by changing either the acquisition flip angle or the repetition time (TR).

So far, quantification of relaxation parameters in ligaments and tendons has focused mostly on the Achilles tendon [3,4,21–23], while only few studies have focused on tendons of the knee [6,24]. It was thus the aim of this work to apply isotropic, 3D, multi-echo UTE imaging with both VFA and VTR techniques to estimate T_1 in the patellar and quadriceps tendons and to compare the extracted values between the two methods. Implementing the sequence as a multi-echo, gradient-echo sequence enabled us to also extract effective transverse relaxation times T_2^*. Due to the isotropic spatial resolution, 3D visualization of the relaxation time parameters of the patellar and quadriceps tendons was facilitated.

2. Material and methods

2.1. T_1 estimation with VFA and VTR

UTE imaging sequences typically use gradient-echo based, FLASH-type, acquisition schemes with short repetition times in combination with low flip-angles for fast acquisition. The equilibrium signal in such sequences is given by:

$$S = M_0 \sin(\alpha)\frac{1 - exp(-TR/T_1)}{1 - exp(-TR/T_1)\cdot cos(\alpha)}\cdot\exp(-TE/T_2^*) \quad (1)$$

with initial magnetization M_0, flip angle α, repetition time TR and echo-time TE. While the three parameters T_1, T_2^*, and M_0 in Eq. (1) are object-specific, the three parameters, TR, TE and α, can be controlled directly via the imaging sequence parameter settings. Considering only data acquired at a particular echo time removes the dependency from T_2^* as a fit parameter and reduces Eq. (1) to an equation containing only two parameters, p_0 and T_1:

$$S(\alpha, TR) = p_0 \sin(\alpha)\frac{1 - exp(-TR/T_1)}{1 - exp(-TR/T_1)\cdot cos(\alpha)} \quad (2)$$

where the terms M_0 and $exp(-TE/T_2^*)$ have been merged together into a single fit parameter p_0. Data acquired with a set of different flip angles in case of VFA or a set of different repetition times in case of the VTR method can then be fitted to Eq. (2) for extracting T_1.

2.2. UTE imaging protocol

A radial 3D-UTE sequence with non-selective hard pulse excitation and center-out spikey-ball trajectory was applied [12]. To avoid digital filtering artifacts affecting the first sampling points, the data sampling was switched on 20 µs before ramping-up the gradients. Constant z-spoiling was applied at the end of each repetition in order to spoil residual magnetization. Multi-echo acquisition was performed in a monopolar fashion during one readout train by using rephasing gradients between the echoes.

Measurements were performed on five volunteers aged between 24 and 50 years old (three male and two female) without known pathologies on a 3 T whole-body MRI scanner (Magnetom PRISMA, Siemens Healthineers, Erlangen, Germany) using a 16-channel NORAS Variety flex coil (NORAS MRI products GmbH, Höchberg, Germany). All volunteers gave written informed consent following the guidelines of the institutional ethics committee. Imaging data were acquired with a field-of-view (FoV) of (160 × 123 × 100) mm^3 and an acquisition matrix size of 80 × 61 × 50, resulting in an isotropic spatial resolution of (2.0 × 2.0 × 2.0) mm^3. For each filled *k*-space, a total of 12,590 radial spokes were acquired with a readout bandwidth of 125 kHz. The duration of the rectangular excitation pulse was 150 µs. VTR acquisition was performed using five different repetitions times of 8 ms, 16 ms, 30 ms, 50 ms and 80 ms, and a constant flip angle of 25°. VFA data were acquired with five different flip angles of 5°, 12°, 20°, 30° and 38°, and TR of 20 ms. Both VTR and VFA protocols acquired 3 echoes with echo-times of 0.10 ms, 2.48 ms and 4.90 ms to allow extracting of T_2^*. The total acquisition time was 63 min (41 min of VTR and 22 min of VFA, respectively). The multi-echo 3D-UTE sequence and the order of the VFA and VTR acquisitions are depicted in Fig. 1.

2.3. Image reconstruction and relaxation parameter fitting

Images were reconstructed offline using MATLAB (The MathWorks, Inc., Natick, Massachusetts, United States of America) using re-gridding with iterative sampling density compensation and an optimized kernel [25]. Using the first echo of the VFA or VTR data series, spatial maps of the T_1 relaxation time were created by fitting the data to Eq. (2) voxel-by-voxel. To extract T_2^* relaxation times, all VFA and VTR datasets were exponentially fitted to corresponding power images computed from the magnitude data [26]. To account for a potential noise bias [27], the squared exponential fitting was performed with an additional offset parameter. Reconstructed mid-sagittal slices from the isotropic 3D-UTE datasets were used to draw regions-of-interest (ROI) manually in the mid-tendon regions of the patellar and quadriceps tendons. The ROIs were drawn on difference images calculated between the first and second echoes, and subsequently applied to both the T_2^* and T_1 maps. The extracted relaxation times were averaged over all voxels of the ROIs and compared between both tendons as well as the VFA and VTR techniques. On average, the ROIs included 38 and 57 voxels for the patella and quadriceps tendon, respectively. Fig. 2 shows the ROIs and the fit curves in the quadriceps tendon for one single subject. Finally, the average relaxation times were used as boundary parameters for the subsequent bivariate histogram analysis.

2.4. Bivariate histogram analysis

Prior to the calculation of bivariate histograms between T_2^* and T_1, the 3D relaxation parameter maps were masked to exclude contributions from noise regions outside the knee. Masking was performed by intensity thresholding of the magnitude image of the first echo, followed by erosion and dilation to remove outliers. To refine the mask, a

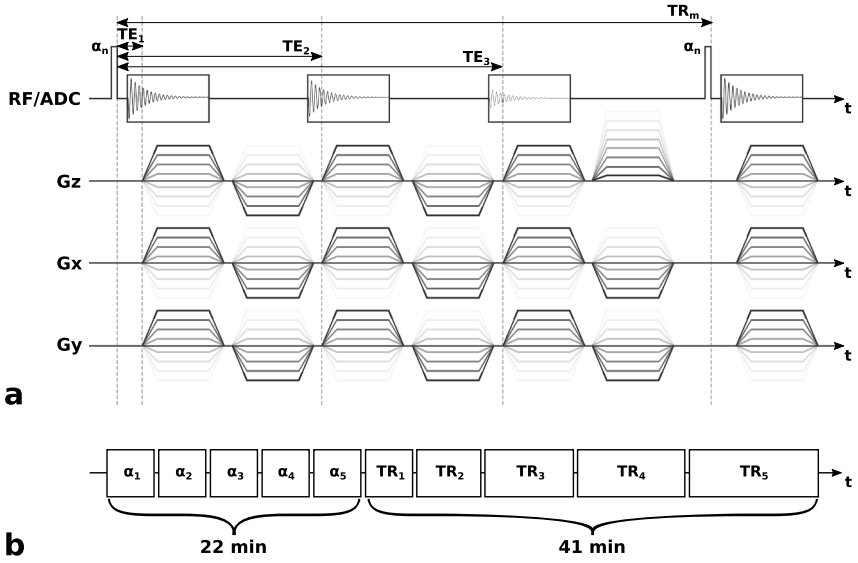

Fig. 1. (a) Sequence diagram depicting the 3D multi-echo UTE acquisition using rectangular excitation pulses with flip angle α_n, echo times TE_1, TE_2 and TE_3, and repetition time TR_m. (b) The course of the experiment showing the order of the different flip angles (VFA method) and repetition times (VTR method).

connectivity analysis was performed to find the connected components in the binary mask with the largest volume. Following extraction of the largest connected component, the resulting binary mask was further processed by closing all holes within the mask with an inverse flood fill operation, i.e., all voxels that cannot be reached by flood filling from the edges of the FoV [28]. The masking process is illustrated for one dataset in Fig. 3.

After masking the 3D relaxation parameter maps, bivariate histograms were calculated by binning the T_1 and T_2^* relaxation times of all voxels into equally sized bins. Because the T_1 relaxation times extracted from the VFA and VTR datasets were very similar (see Fig. 4), only the T_1 values from the VFA method were used for creating the histogram as this method has a shorter acquisition time and is therefore better suited for clinical applications. Clearly visible clusters in the histograms were manually

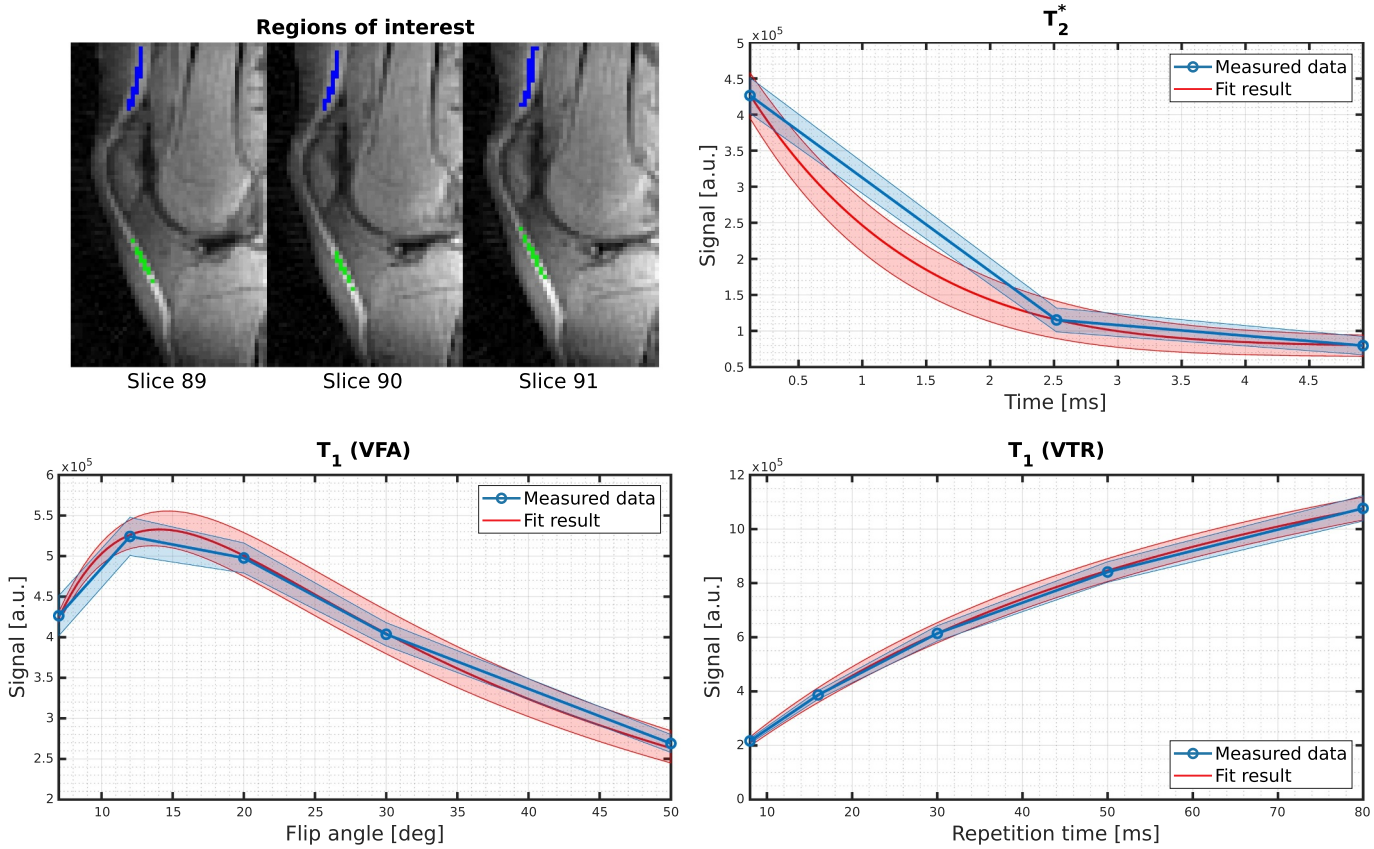

Fig. 2. Placement of tendon ROIs in a single subject for the quadriceps (blue) and patellar (green) tendons (*upper left*). The three plots show the measured signal and the fit results for T_2^* (*upper right*), T_1 (VFA) (*lower left*) and T_1 (VTR) fitting (*lower right*), averaged over the ROIs of the quadriceps tendon. The colored bands depict the standard deviation over the ROIs.

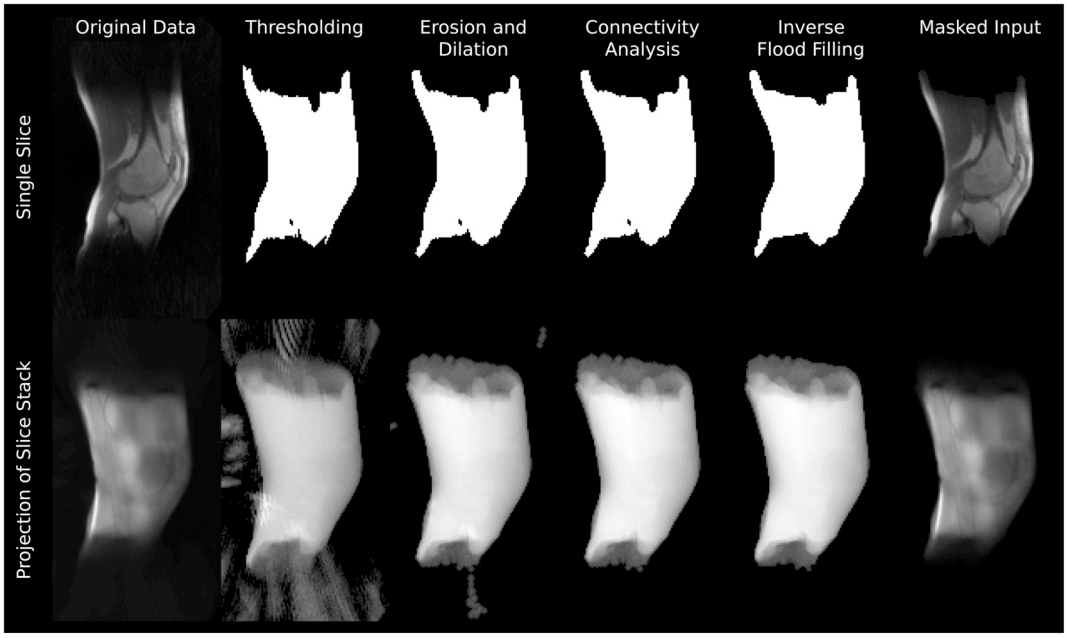

Fig. 3. Illustration of the masking process for the input data to remove outliers prior to bivariate histogram calculation. (*Top row*) Processing steps for obtaining masked data, including thresholding, erosion and dilation, connectivity analysis and inverse flood filling, applied to a single slice. (*Bottom row*) Results of the individual processing steps projected over the entire slice stack.

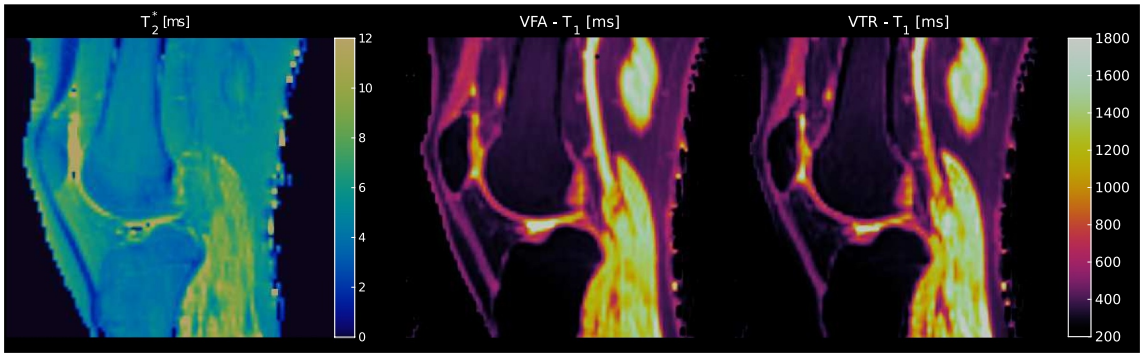

Fig. 4. *Left:* T_2^*-map of a single subject, scaled between 0 ms and 12 ms. *Middle and right*: T_1-maps of the same subject, scaled between 100 ms and 1800 ms, for both the VFA and the VTR methods, respectively. In both maps the patellar and the quadriceps tendons are easily identified by their different relaxation times to the surrounding tissues.

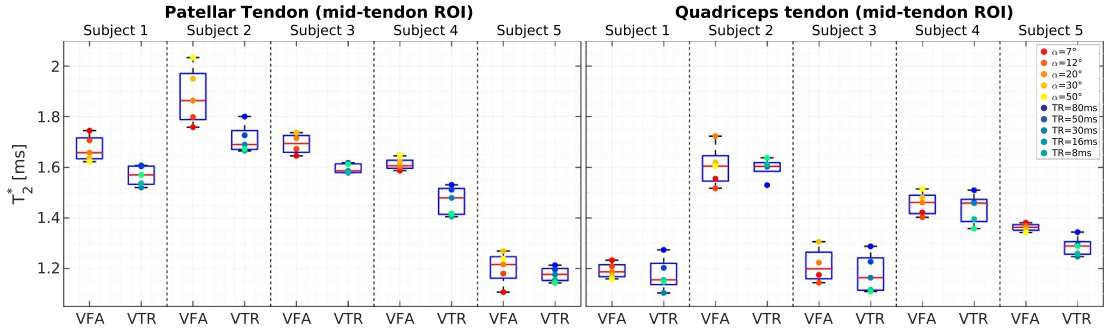

Fig. 5. Box plots of the T_2^* relaxation times derived from manually drawn ROIs in the patellar and quadriceps mid-tendons, obtained from all multi-echo 3D-UTE acquisitions with different flip angles (VFA) and repetition times (VTR).

outlined by drawing ROIs around them, and subsequently visualized using 3D surface reconstruction. To improve the masks resulting from this histogram analysis and to remove outliers, a connectivity analysis similar to that described above was performed prior to visualization, retaining only the largest connected components of the masks. Since no prominent cluster was found in the bivariate histogram located in the range of the extracted T_1 and T_2^* times of the patellar and quadriceps tendons, a ROI was placed in the histogram encompassing a rectangular region in the ranges of 1.0 ms < T_2^* < 3.0 ms and 350 ms < T_1 < 900 ms. Finally, the masks of those cluster ROIs corresponding to bone marrow and the patellar and quadriceps tendons were visualized using a T_1- and T_2^*-based color-encoded semi-transparent 3D volumetric rendering.

3. Results

As shown in Fig. 4, both the patellar and quadriceps tendons were clearly identifiable on the calculated T_2^* maps due to their short T_2^* relaxation times. Since the longest echo-time acquired was only 4.9 ms, the numerical values obtained for other tissues with longer T_2^* relaxation time constants are more uncertain and likely underestimated and should thus be compared with caution to values from the literature. By comparing the inter-individual mean T_2^* values, extracted from the manually drawn ROIs in the mid-tendons, for a wide range of acquisition parameters of the VTR and VFA approach (Fig. 5), several effects are observed: (1) the patellar tendon reveals a broader inter-individual variation of T_2^* values (ranging from 1.2 ms to 1.9 ms) compared to the quadriceps tendon with a range of 1.2 ms to 1.6 ms; (2) averaged over the VFA and VTR acquisitions and all subjects, the mean T_2^* of the quadriceps tendon is slightly lower (1.4 ms ± 0.2 ms) compared to the patellar tendon (1.6 ms ± 0.2 ms); (3) for the different flip angles and repetition times, the intra-individual T_2^* variation was up to 15% for VFA and 9% for VTR, suggesting only small multi-compartment effects on T_2^* within the tendons; (4) in the patellar tendon, the VFA-based T_2^* values were slightly higher compared to the VTR-based results.

Fig. 4 also displays maps of the T_1 relaxation times for both methods. Both the quadriceps and patellar tendons have distinctly different T_1 relaxation times compared to their surrounding tissues, making it easy to identify them. The visual appearance as well as the numerical T_1 values of the tendons derived from the mid-tendon ROIs are comparable between the two methods, with the T_1 values obtained with the VFA method being slightly higher than those obtained with the VTR method. The mean mid-tendon T_1 values of the patellar tendon, averaged over all subjects, were 501 ms ± 67 ms and 453 ms ± 59 ms for the VFA and VTR acquisitions, respectively. Compared to the patellar tendon, the quadriceps mid-tendon had higher mean T_1 values of 716 ms ± 131 ms and 670 ms ± 82 ms for VFA and VTR, respectively. The differences in T_1 between the patellar and quadriceps mid-tendon ROIs were statistically significant ($p < 0.05$) in a two-sided Wilcoxon rank sum test with p-values of 0.02 (VFA) and 0.01 (VTR), respectively.

The bivariate histogram (Fig. 6) revealed several well-delineated clusters, exhibiting similar relaxation parameters in the range of 150 ms < T_1 < 450 ms and 3 ms < T_2^* < 7 ms. Also visible is a broader cluster in the range of 800 ms < T_1 < 1500 ms and 5 ms < T_2^* < 11 ms. In the specific relaxation time range for the patellar and quadriceps tendons, estimated from the previous mid-tendon ROI analysis (1.5 ms < T_2^* < 2.5 ms and 400 ms < T_1 < 850 ms), no distinct clusters were visible. By separating and masking the bivariate histogram, the tissue types underlying the clusters became evident (Fig. 7). The narrow and sharp clusters between 150 ms < T_1 < 450 ms and 3 ms < T_2^* < 7 ms mainly reflect bone marrow (Fig. 7, blue), as well as fat and skin (Fig. 7, green), while the broader cluster with higher T_1 values (Fig. 7, yellow) can be primarily attributed to muscle tissue. By placing an ROI in the range of 1.0 ms < T_2^* < 3.0 ms and 350 ms < T_1 < 900 ms in the bivariate histogram, the patellar and quadriceps tendons could also be extracted (Fig. 7, red). The boundaries of this ROI were extended from the previously obtained mid-tendon values to allow inclusion of more voxels in the transitory regions of the tendons, specifically the patella and tibia entheses.

Average relaxation parameter distributions obtained after segmenting the entire tendon volumes from the bivariate histograms are shown as box plots in Fig. 8 and Fig. 9 for T_2^* and T_1, respectively. Compared to the ROI-based, mid-tendon results (see Fig. 4), the volume-averaged T_2^* values show less variation between both subjects and methods. The mean T_2^* value in the patellar tendon was 1.8 ms ± 0.1 ms, which was again longer compared to the quadriceps tendon (mean T_2^* = 1.4 ms ± 0.2 ms). Overall, volume-based mean T_2^* values were approximately 10% to 15% larger compared to ROI-based mid-tendon results.

Volume-based, average T_1 relaxation times were 527 ms ± 42 ms (VFA) and 476 ms ± 40 ms (VTR) in the patellar tendon, and 662 ms ± 97 ms (VFA) and 637 ms ± 40 ms (VTR) in the quadriceps tendon. Again, the VTR method consistently resulted in shorter T_1 relaxation times compared to the VFA method. Compared to the mid-tendon ROI analysis, the T_1 relaxation times averaged over the entire tendon volume were comparable within 10%.

Based on the segmentation of the patellar and quadriceps tendons (Fig. 7, red), a color-coded 3D volumetric rendering was created to visualize the distributions of T_1 and T_2^* values over the entire tendon volume (Fig. 10), including parts of the tendons entheses. Inspection of these volumetric renderings indicates that T_1 is not constant over the volume of the tendons but contains “hot spots” in some subjects as well as an increase in the relaxation time towards the entheses. On the other hand, T_2^* shows stronger variations between subjects, which may be related to magic angle effects [2,22] due to possible different knee orientations with respect to B_0. Another reason for these higher variations could be partial volume effects due to the limited spatial resolution.

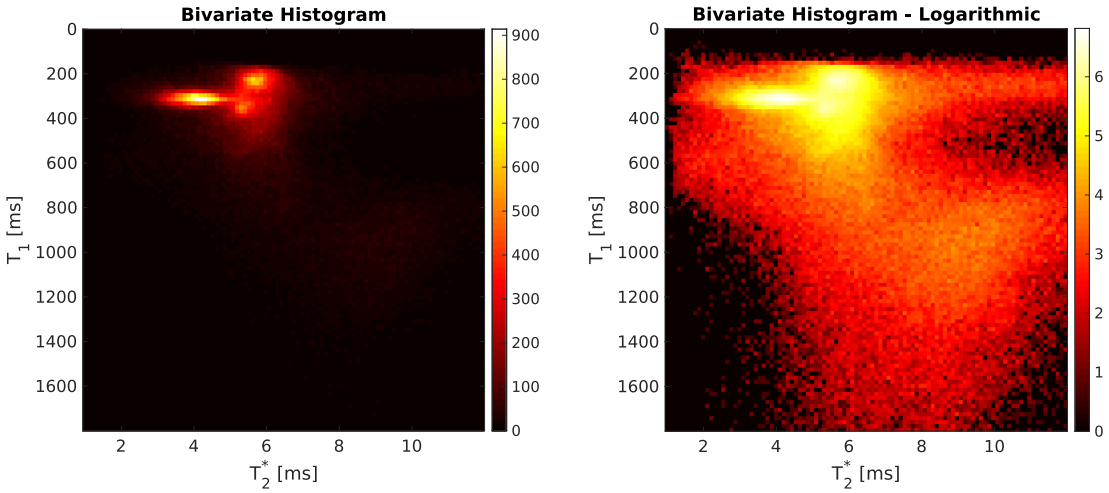

Fig. 6. Bivariate histogram (*left*) and logarithmically-scaled bivariate histogram (*right*) of T_1 and T_2^* showing the color-coded number of voxels corresponding to the respective relaxation times. Several clusters are identifiable in the histogram on the left, corresponding to different tissues. The logarithmic scaling on the right visualizes broader clusters otherwise hidden in the background.

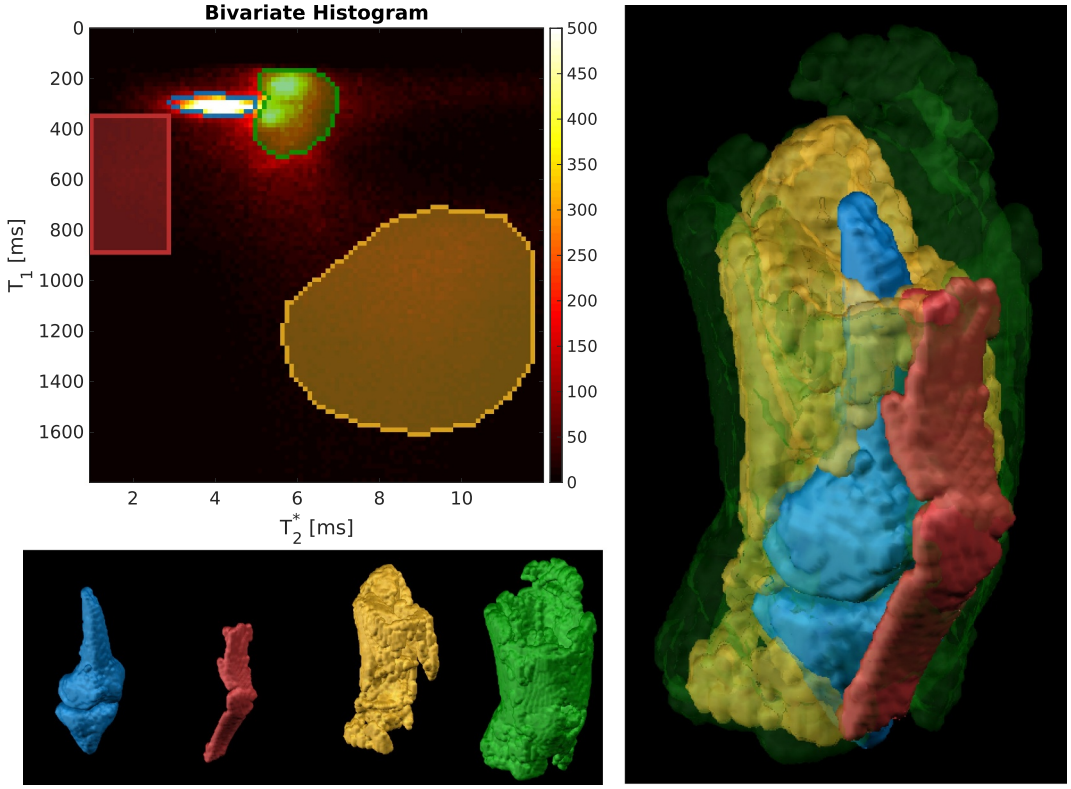

Fig. 7. Based on the bivariate histogram displayed in Fig. 6, clusters were manually selected (*top left*) and visualized as a 3D surface (*bottom left*). The colors correspond to bone marrow (blue), patellar and quadriceps tendons (red), muscle (yellow), as well as skin and other fatty tissue (green). On the right, a combination of all extracted surfaces is shown.

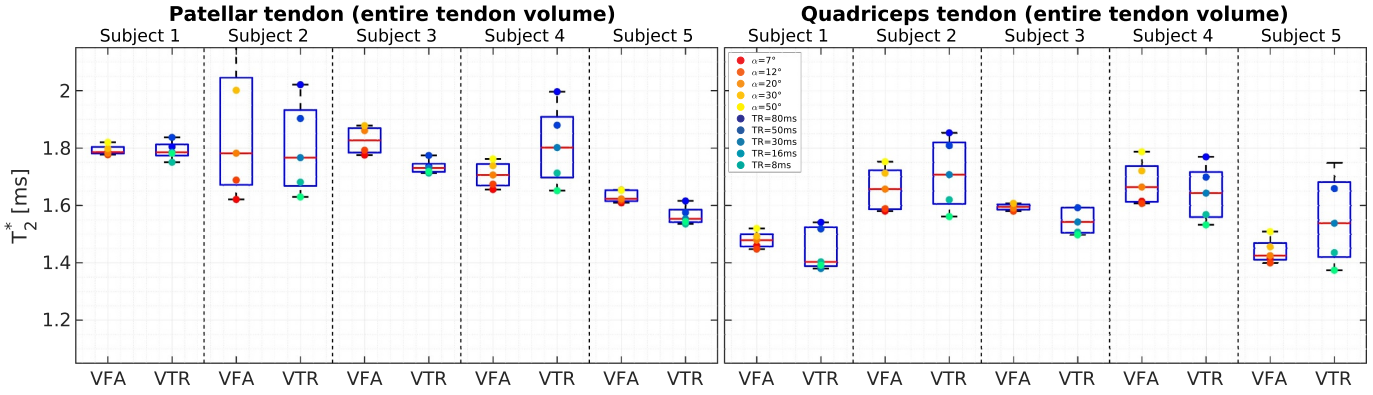

Fig. 8. Box plots of the T_2^* relaxation times, averaged over the entire patellar and quadriceps tendons after segmentation, and obtained from all multi-echo 3D-UTE acquisitions with different flip angles (VFA) and repetition times (VTR).

4. Discussion

The mean T_2^* relaxation time of 1.8 ms for the patellar tendon is comparable with the only known literature reference of 2.0 ms [4]. Similar to the current work, data in that study had also been acquired in vivo and with a 3 T field strength. Although it is conceivable that different tendons in the body should have comparable T_2^* relaxation times, no reference data could be found in the literature for the quadriceps tendon. With T_2^* being much longer than the duration of the short rectangular rf-pulse used for excitation (1.8 ms ≫ 0.15 ms), relaxation effects during the rf-pulse [19,29] should be negligible for the analysis of the VFA and VTR data in estimating T_1. The observed differences in T_2^* between the VFA and VTR methods in the patellar tendon (Fig. 5) might be related to subject motion and partial volume effects due to the limited spatial resolution. Since the datasets were acquired sequentially, even small movements of the subjects between the scans can cause changes in T_2^* as the ROIs shift out of their mid-tendon position. This effect should be more pronounced with the patellar tendon as it is thinner than the quadriceps tendon and thus more susceptible to motion. The higher volume averaged T_2^* values compared to the mid-tendon ROI analysis might be related to the decreases of T_2^* towards the center of the tendons. The intra-individual variation of T_2^* with changing flip angle (VFA) or repetition time (VTR) indicates the presence of multiple compartments with different T_1 relaxation times. Such compartments could be collagen bound water and free water, having different T_1 and T_2^* relaxation times. However, the overall influence of the different T_1 weightings on T_2^* was <15% of the mean T_2^* for all subjects and measurements.

Since the VTR and VFA techniques both resulted in comparable T_1 relaxation times in both tendons, future studies are likely to favor the

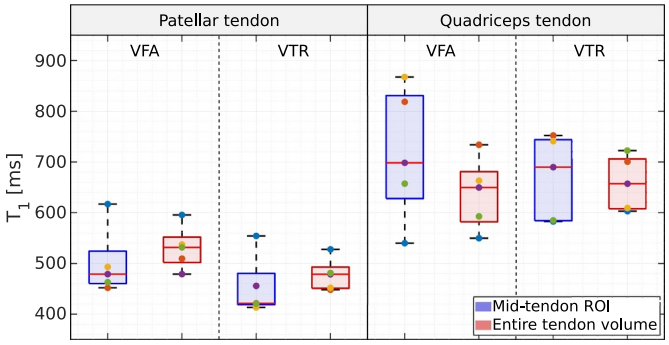

Fig. 9. Comparison between T_1 relaxation times obtained from VFA and VTR in the mid-tendon regions (blue) of the patellar (*left*) and quadriceps tendon (*right*) and the entire tendon volumes after segmentation (red).

VFA technique due to its shorter acquisition time. Due to the already long total acquisition time, we restricted the maximum TR in our study to 80 ms with the VTR technique. Considering that the T_1 relaxation times in both tendons are significantly longer, more extended TRs would have been necessary for optimal sampling of the T_1 saturation recovery curves with VTR. Consequently, the T_1 relaxation times obtained with the VTR technique in our study are most likely underestimated, especially since additional water compartments with longer T_1 relaxation times might exist in tendons. This assumption of underestimation is further supported by the fact that the VFA-based T_1 values were slightly longer for both tendons and all subjects than the VTR results. The VTR technique, on the other hand, could be of advantage when performing T_1 mapping on high field (preclinical) systems, for which the rf-pulse performance may be inferior regarding stability of flip-angles or B_1 inhomogeneity effects may be stronger. In the present study, B_1 inhomogeneities were not taken into account for several reasons. Mapping of B_1 in tendons or tissues with very short T_2^* relaxation times is generally challenging because standard B_1 mapping techniques [30–32] do not show signal in such tissues and calibrate their flip angles consequently on long T_2 tissues, or require very long TRs, which are impractical for isotropic 3D acquisitions. One promising approach for B_1 mapping is the actual flip angle imaging (AFI) method [33,34], which uses an interleaved acquisition with two different repetition times. This method has only recently been demonstrated to work with 3D UTE acquisition; however, with an anisotropic resolution [24,35]. A major limitation of UTE-AFI based B_1 mapping is a highly prolonged total acquisition time when applied with isotropic high resolution, as is advantageous for 3D segmentation and visualization. Because B_1 inhomogeneities were not corrected in this study, the obtained T_1 values of the patellar and quadriceps tendon could be over- or underestimated, where the over- or underestimation may also depend on blurring from surrounding tissues and chemical shift artifacts.

The only known reference data for T_1 values in the patellar and quadriceps tendons are 656 ± 43 ms and 800 ± 66 ms, respectively [24]. While comparable, these values are slightly higher than those found in the current study. As outlined above, these differences are likely due to the application of B_1 correction based on UTE-AFI in ref. [24], which could result in increased T_1 values. Another reason for the discrepancy may be ROI placement. As demonstrated by the 3D visualization (Fig. 10), T_1 varies within the tendons on the individual level, implying that placement and size of ROIs can affect the mean values. The differences in T_1 between both tendons could be due to the fact that the patellar tendon is a ligament connecting bone to bone (i.e., patella to tibia), whereas the quadriceps tendon connects bone to muscle (patella to quadriceps). Available 3D segmentation techniques, and thus 3D mapping of T_1 and T_2^* distributions, should enable future studies to investigate physiological influences, such as age, physical training or pathologies, on changes in these distributions of relaxation parameters over the entire tendon volume.

The bivariate histogram analysis of the relaxation time maps applied in the present work is limited by three major factors. First, only three echoes with short echo times (4.9 ms being the longest) were acquired, from which T_2^* was estimated. This could have resulted in underestimation of the values derived for tissues with longer T_2^* relaxation times, and therefore, caused the clusters in the histogram to be

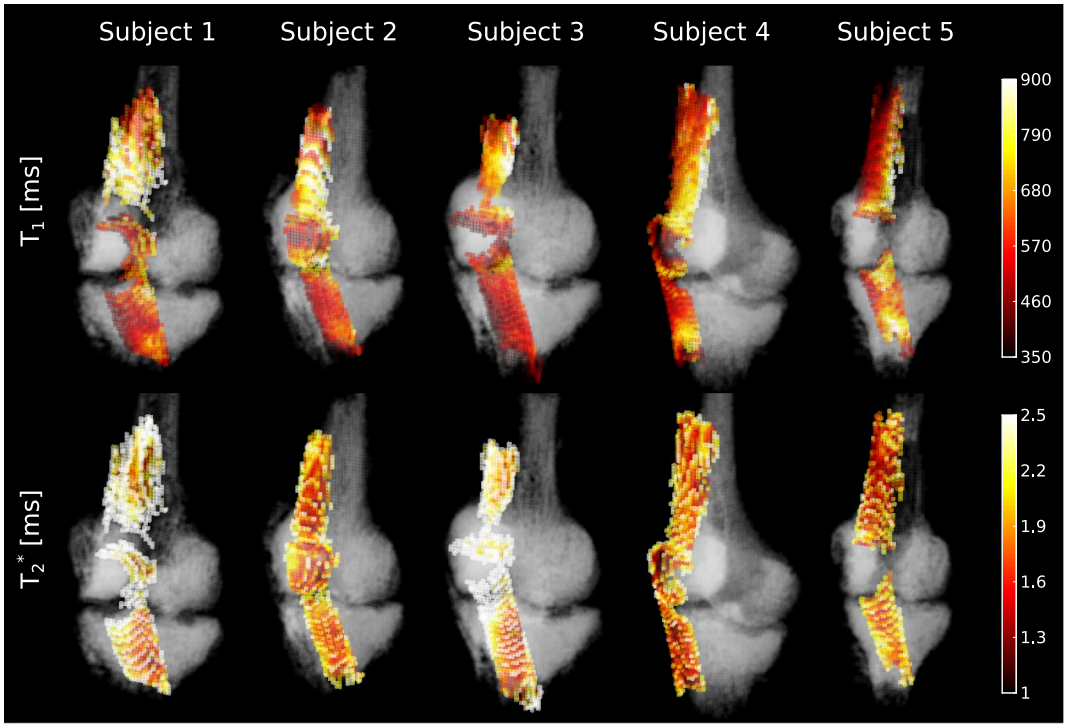

Fig. 10. Color-coded volumetric 3D renderings of T_1 (*top*) and T_2^* (*bottom*) for all five subjects. For geometrical reference, the segmented bones are also shown semi-transparently with gray levels.

compressed in the range along the T_2^* axis. Second, the spatial resolution of $2.0 \times 2.0 \times 2.0\,mm^3$ is relatively low, which is due to the fact that both VFA and VTR were acquired for comparing the T_1 mappings, and total measurement time was limited to approximately 1 h to reduce motion between separate scans with different flip angles and TRs. Future experiments should not only omit the VTR scan entirely, but should also combine the 3D-UTE acquisition and reconstruction with acceleration techniques, such as SENSE [36,37] or compressed sensing [38], to benefit from reduced scan time and increased spatial resolution. Lastly, by combining the VFA acquisition with B_1 mapping and inhomogeneity compensation, and using advanced shimming for B_0 homogenization, the extent of the T_1 and T_2^* clusters in the bivariate histogram may be reduced, potentially leading to a more robust and fully-automatic 3D segmentation.

By comparing the relaxation times obtained from the manually drawn mid-tendon ROIs with the values averaged over the segmented tendon volume, we could show that placement of ROIs is crucial for obtaining consistent and trustworthy results. Although the obtained relaxation times were comparable for both T_2^* and T_1, the inter-individual variations were reduced by averaging over the entire segmented tendon volumes. Variations in the mid-tendon ROIs might have been caused by partial volume effects, motion between the separate VFA and VTR scans or by errors in drawing the manual ROIs.

In conclusion, we have demonstrated similar T_1 relaxation parameters extracted from 3D-UTE VFA and VTR acquisitions for knee tendons, and contributed additional reference data to the currently sparse literature regarding relaxation times in the quadriceps and patellar tendons. Furthermore, by combining 3D isotropic T_1 and T_2^* mapping of the entire knee with a bivariate histogram analysis, we were able to segment the quadriceps and patellar tendons, and visualize the relaxation parameter distributions over the entire tendon volume.

Acknowledgments

This work was supported by the German Research Foundation (DFG, DU 298/25-1, RE 1123/22-1, ZA 592/4-1) and the Interdisciplinary Center for Clinical Research (IZKF, J64) in Jena, Germany. The authors have no relevant financial conflicts to disclose with regard to this study.

References

[1] Cook JL, Khan KM, Purdam CR. Conservative treatment of patellar tendinopathy. Phys Ther Sport 2001;2(2):54–65. https://doi.org/10.1054/ptsp.2001.0069.
[2] Fullerton GD, Rahal A. Collagen structure: the molecular source of the tendon magic angle effect. J Magn Reson Imaging 2007;25(2):345–61. https://doi.org/10.1002/jmri.20808.
[3] Jerban S, Nazaran A, Cheng X, Carl M, Szeverenyi N, Du J, et al. Ultrashort echo time T2 ∗ values decrease in tendons with application of static tensile loads. J Biomech 2017;61:160–7. https://doi.org/10.1016/j.jbiomech.2017.07.018.
[4] Grosse U, Springer F, Hein T, Grözinger G, Schabel C, Martirosian P, et al. Influence of physical activity on T1 and T_2^* relaxation times of healthy achilles tendons at 3T. J Magn Reson Imaging 2015;41(1):193–201. https://doi.org/10.1002/jmri.24525.
[5] Grosse U, Syha R, Hein T, Gatidis S, Grözinger G, Schabel C, et al. Diagnostic value of $T_{1\,1}$ and T_2^* relaxation times and off-resonance saturation effects in the evaluation of achilles tendinopathy by MRI at 3T: MR evaluation of Achilles tendinopathy. J Magn Reson Imaging 2015;41(4):964–73. https://doi.org/10.1002/jmri.24657.
[6] Kijowski R, Wilson JJ, Liu F. Bicomponent ultrashort echo time T_2^* analysis for assessment of patients with patellar tendinopathy. J Magn Reson Imaging 2017;46(5):1441–7. https://doi.org/10.1002/jmri.25689.
[7] Robson MD, Gatehouse PD. Consequences of T2 relaxation during half-pulse slice selection for ultrashort TE imaging. Magn Reson Med 2010;64(2):610–5. https://doi.org/10.1002/mrm.22323.
[8] Josan S, Pauly JM, Daniel BL, Pauly KB. Double half RF pulses for reduced sensitivity to eddy currents in UTE imaging. Magn Reson Med 2009;61(5):1083–9. https://doi.org/10.1002/mrm.21879.
[9] Rahmer J, Börnert P, Groen J, Bos C. Three-dimensional radial ultrashort echo-time imaging with T2 adapted sampling. Magn Reson Med 2006;55(5):1075–82. https://doi.org/10.1002/mrm.20868.
[10] Rahmer J, Blume U, Börnert P. Selective 3D ultrashort TE imaging: comparison of "dual-echo" acquisition and magnetization preparation for improving short-T2 contrast. Magn Reson Mater Phys Biol Med 2007;20(2):83–92. https://doi.org/10.1007/s10334-007-0070-6.
[11] Krämer M, Motaal AG, Herrmann K-H, Löffler B, Reichenbach JR, Strijkers GJ, et al. Cardiac 4D phase-contrast CMR at 9.4 T using self-gated ultra-short echo time (UTE) imaging. J Cardiovasc Magn Reson 2017;19(1):39. https://doi.org/10.1186/s12968-017-0351-9.
[12] Herrmann K-H, Krämer M, Reichenbach JR. Time efficient 3D radial UTE sampling with fully automatic delay compensation on a clinical 3T MR scanner. Fan X, editor. PLOS ONE 2016;11(3):e0150371. https://doi.org/10.1371/journal.pone.0150371.
[13] Koff MF, Powonder SL, Shah PH, Yang LW, Potter HG. Ultrashort echo imaging of cyclically loaded rabbit patellar tendon. J Biomech 2014;47(13):3428–32. https://doi.org/10.1016/j.jbiomech.2014.08.018.
[14] Chang EY, Du J, Iwasaki K, Biswas R, Statum S, He Q, et al. Single- and Bi-component T_2^* analysis of tendon before and during tensile loading, using UTE sequences: T_2^* Analysis of Tendon With Tension. J Magn Reson Imaging 2015;42(1):114–20. https://doi.org/10.1002/jmri.24758.
[15] Zhu DC, Penn RD. Full-brain T1 mapping through inversion recovery fast spin echo imaging with time-efficient slice ordering. Magn Reson Med 2005;54(3):725–31. https://doi.org/10.1002/mrm.20602.
[16] Deichmann R, Hahn D, Haase A. Fast T1 mapping on a whole-body scanner. Magn Reson Med 1999;42(1):206–9. https://doi.org/10.1002/(SICI)1522-2594(199907)42:1<206::AID-MRM28>3.0.CO;2-Q.
[17] Ordidge RJ, Gibbs P, Chapman B, Stehling MK, Mansfield P. High-speed multislice T_1 mapping using inversion-recovery echo-planar imaging. Magn Reson Med 1990;16(2):238–45. https://doi.org/10.1002/mrm.1910160205.
[18] Fram EK, Herfkens RJ, Johnson GA, Glover GH, Karis JP, Shimakawa A, et al. Rapid calculation of T1 using variable flip angle gradient refocused imaging. Magn Reson Imaging 1987;5(3):201–8. https://doi.org/10.1016/0730-725X(87)90021-X.
[19] Springer F, Steidle G, Martirosian P, Syha R, Claussen CD, Schick F. Rapid assessment of longitudinal relaxation time in materials and tissues with extremely fast signal decay using UTE sequences and the variable flip angle method. Invest Radiol 2011;46(10):610–7. https://doi.org/10.1097/RLI.0b013e31821c44cd.
[20] Du J, Bydder GM. Qualitative and quantitative ultrashort-TE MRI of cortical bone. NMR Biomed 2013;26(5):489–506. https://doi.org/10.1002/nbm.2906.
[21] Wellen J, Helmer KG, Grigg P, Sotak CH. Spatial characterization of T1 andT2 relaxation times and the water apparent diffusion coefficient in rabbit Achilles tendon subjected to tensile loading. Magn Reson Med 2005;53(3):535–44. https://doi.org/10.1002/mrm.20361.
[22] Du J, Chiang AJ-T, Chung CB, Statum S, Znamirowski R, Takahashi A, et al. Orientational analysis of the Achilles tendon and enthesis using an ultrashort echo time spectroscopic imaging sequence. Magn Reson Imaging 2010;28(2):178–84. https://doi.org/10.1016/j.mri.2009.06.002.
[23] Wengler K, Tank D, Fukuda T, Paci JM, Huang M, Schweitzer ME, et al. Diffusion tensor imaging of human Achilles tendon by stimulated echo readout-segmented EPI (ste-RS-EPI). Magn Reson Med 2018;80(6):2464–74. https://doi.org/10.1002/mrm.27220.
[24] Ma Y-J, Zhao W, Wan L, Guo T, Searleman A, Jang H, et al. Whole knee joint T $_1$ values measured in vivo at 3T by combined 3D ultrashort echo time cones actual flip angle and variable flip angle methods. Magn Reson Med 2019;81(3):1634–44. https://doi.org/10.1002/mrm.27510.
[25] Zwart NR, Johnson KO, Pipe JG. Efficient sample density estimation by combining gridding and an optimized kernel. Magn Reson Med 2012;67(3):701–10. https://doi.org/10.1002/mrm.23041.
[26] Miller AJ, Joseph PM. The use of power images to perform quantitative analysis on low SNR MR images. Magn Reson Imaging 1993;11(7):1051–6. https://doi.org/10.1016/0730-725X(93)90225-3.
[27] Henkelman RM. Measurement of signal intensities in the presence of noise in MR images: technical reports: signal intensities in MR image noise. Med Phys 1985;12(2):232–3. https://doi.org/10.1118/1.595711.
[28] M. Krämer, B. Herzau, J.R. Reichenbach, Segmentation and visualization of the human cranial bone by T_2^* approximation using ultra-short echo time (UTE) magnetic resonance imaging. Z Med Phys; Epub ahead of print, https://doi.org/10.1016/j.zemedi.2019.06.003.
[29] Springer F, Steidle G, Martirosian P, Claussen CD, Schick F. Effects of in-pulse transverse relaxation in 3D ultrashort echo time sequences: analytical derivation, comparison to numerical simulation and experimental application at 3T. J Magn Reson 2010;206(1):88–96. https://doi.org/10.1016/j.jmr.2010.06.010.
[30] Klose U. Mapping of the radio frequency magnetic field with a MR snapshot FLASH technique. Med Phys 1992;19(4):1099–104. https://doi.org/10.1118/1.596828.
[31] Insko EK, Bolinger L. Mapping of the radiofrequency field. J Magn Reson A 1993;103(1):82–5. https://doi.org/10.1006/jmra.1993.1133.
[32] Chung S, Kim D, Breton E, Axel L. Rapid B1 + mapping using a preconditioning RF pulse with Turbo FLASH readout. Magn Reson Med 2010;64(2):439–46. https://doi.org/10.1002/mrm.22423.
[33] Yarnykh VL. Actual flip-angle imaging in the pulsed steady state: a method for rapid three-dimensional mapping of the transmitted radiofrequency field. Magn Reson Med 2007;57(1):192–200. https://doi.org/10.1002/mrm.21120.
[34] Nehrke K. On the steady-state properties of actual flip angle imaging (AFI). Magn Reson Med 2009;61(1):84–92. https://doi.org/10.1002/mrm.21592.
[35] Ma Y-J, Lu X, Carl M, Zhu Y, Szeverenyi NM, Bydder GM, et al. Accurate T $_1$ mapping of short T $_2$ tissues using a three-dimensional ultrashort echo time cones actual flip angle imaging-variable repetition time (3D UTE-Cones AFI-VTR) method. Magn Reson Med 2018;80(2):598–608. https://doi.org/10.1002/mrm.27066.
[36] Pruessmann KP, Weiger M, Scheidegger MB, Boesiger P. SENSE: sensitivity encoding for fast MRI. Magn Reson Med 1999;42(5):952–62. https://doi.org/10.1002/(SICI)1522-2594(199911)42:5<952::AID-MRM16>3.0.CO;2-S.
[37] Pruessmann KP, Weiger M, Börnert P, Boesiger P. Advances in sensitivity encoding with arbitrary *k* -space trajectories. Magn Reson Med 2001;46(4):638–51. https://doi.org/10.1002/mrm.1241.
[38] Lustig M, Donoho D, Pauly JM. Sparse MRI: the application of compressed sensing for rapid MR imaging. Magn Reson Med 2007;58(6):1182–95. https://doi.org/10.1002/mrm.21391.